

Ultra-long Fe nanowires by pulsed electrodeposition with full filling of alumina templates

J Azevedo^{1,2}, C T Sousa¹, J Ventura¹, A Apolinario¹, A Mendes² and

J P Araujo¹

¹ IFIMUP and IN-Institute of Nanoscience and Nanotechnology and Departamento de Física e Astronomia, Universidade do Porto, Rua do Campo Alegre 687, 4169-007 Porto, Portugal

² LEPABE-Faculdade de Engenharia, Universidade do Porto, Rua Dr. Roberto Frias, 4200-465 Porto, Portugal

E-mail: jearaujo@fc.up.pt

Abstract

With the increasing demand for high quality methods for the fast fabrication of extremely high aspect ratio nanoparticles, the research for efficient, low-cost and simple techniques has become fundamental. A promising approach on the synthesis of these materials is here addressed. Pulsed electrodeposition in porous anodic alumina templates was improved enabling, for the first time, a simple and cost effective fabrication method for vertically aligned nanomaterials with aspect ratios never reported with this method. Iron nanowires were electrodeposited and the effect of electrolyte molar concentration, temperature and stirring, pulse shape and barrier layer thickness on the deposition quality was investigated to potentially increase the template filling and the nanowires length. The electro-deposition temperature and current density were also found to be determinant parameters affecting NWs crystallography. A methodology of surface response design of experiment was conducted to retrieve the optimum values for the deposition parameters. With the determined optimized process, we were able to obtain filling ratios up to 93% and aspect ratios over 10 times higher than previous reports for an alternating current method. The high deposition homogeneity combined with the simplicity of the pulsed deposition method, can open new opportunities for the nanofabrication of nanowires.

Keywords: pulsed electrodeposition, ultra-long nanowires, high aspect ratio nanoparticles, porous anodic alumina templates, response surface methods

1. Introduction

Vertically aligned magnetic nanowires (NWs) are expected to play a major role in future nanotechnologies due to their high aspect ratio, small-size and quantum effects that can greatly modify the physical and chemical properties from their bulk counterparts. In the case of iron (Fe) NWs, such properties generated great interest for a wide range of applications, such as high-density perpendicular magnetic recording media, chemical and biological sensors and microelectromechanical systems [1–5]. Within the numerous methods of fabrication, template assisted deposition within porous anodic alumina (PAA) has been widely used to prepare large

arrays of vertically oriented metallic NWs [6–9]. The ability to tailor the PAA template morphology, combined with the simplicity and low cost of the electrodeposition methods available to fill them, makes this technique ideal for industrial applications. Although the electrodeposition of Fe NWs in PAA templates dates back 20 years [9], the main problem concerning the uniform filling of long templates remains unsolved. To our knowledge, only low thickness (few micrometers) templates have been used to fabricate Fe NWs and with filling fractions far from 100%. In this work we focus on the electrodeposition of Fe NWs inside alumina templates synthesized with oxalic acid (standard conditions [10]).

The electrodeposition process, uses an electrical current to reduce cations in solution to metal forming a metallic coating [11]. Using PAA as template presents a challenge because the interface between the metallic aluminum substrate and the nanopores is a thick layer of alumina (~52 nm). Alumina is a good dielectric [12], and storing the electric charge creates an electrical field that blocks the current flow and storing the electric charges to create an electrical field [8]. There are two approaches to overcome this limitation depending whether the applied electric current is constant (dc) or alternate (ac). The first, to avoid charging the dielectric barrier, requires the removal of the bottom insulator, and therefore of the Al substrate, followed by the deposition of a metallic contact (usually Au) [3, 5, 13–16]. This method presents major disadvantages such as an elaborate fabrication procedure and the difficulty of manipulating templates thinner than 20 μm [15]. On the other hand, ac methods only require the reduction of the barrier layer thickness (δ_b) to perform deposition, given the alternate polarization pulse that allows discharging the alumina capacitance. The most common approach to reduce δ_b is to perform a pore widening process in a bath containing phosphoric acid (H_3PO_4) at 30 °C [1, 3, 17–19]. For the particular case of the electrodeposition of Fe NWs, both methods have been reported. However, achieving large pore fillings in PAA templates thicker than few micrometers either required a too laborious process (dc) or was limited by hydrogen formation, due to the high cathodic potentials and the slow diffusion transport of the ionic species inside the PAA pores (ac) [20].

Recent results demonstrated [8, 10, 21–23] that pulsed electrodeposition (PED), is an excellent alternative to the two previous methods. In PED, the reduction of the PAA barrier layer is not performed by chemical etching, which isotropically attacks the alumina, hence reducing the wall and barrier layer thickness alike, usually leading to low PAA homogeneity. A different approach relies on the linear dependence between the anodization voltage and pore diameter, inter pore distance and δ_b [20, 23–25] (0.85 nm V^{-1} , 2.77 nm V^{-1} and 1.29 nm V^{-1} , respectively, for the used pH, temperature and electrolyte) [26]. This method allows reducing the barrier layer thickness without changing the diameter of the main pore [8, 10]. Using a non-steady-state anodization we were able to accurately tune δ_b by controlling the final anodization voltage. By exponentially reducing V_{ap} , δ_b is significantly reduced, achieving nominal values as low as ~4 nm for $V_{\text{ap}} \approx 3$ V, giving origin to a dendritic structure at the bottom of the template without changing the characteristic PAA nanopore dimensions. This enables the deposition current to flow through such a small insulating layer [10]. Also, in contrast with typical square wave ac deposition, a modulated electric pulse is applied and a rest pulse is introduced to counterbalance the slow ionic diffusion and restore the metallic ions concentration at the deposition interface, leading to a more uniform NW growth [8, 10, 20, 27].

In this work, for the first time, we address the influence and optimization of the main pulsed electrodeposition parameters (current density and rest pulse duration; electrolyte temperature, molar concentration and stirring; and barrier layer thickness) on the Fe NWs fabrication aiming

uniform filling of long membranes. Afterwards, a cross parameter study was performed, allowing us to reach the optimum pore filling conditions with which templates with 20 μm length are almost completely filled (93%), preserving high pore filling values up to 50 μm .

2. Sample preparation and characterization

PAA templates were fabricated from Alfa Aesar high purity 0.25 mm thick Al foil (99.997%). Each Al foil was rinsed in acetone, ethanol and distilled water. Immediately prior to anodization, the Al foils were individually electropolished in a stirred 10 $^{\circ}\text{C}$ bath of perchloric acid, HClO_4 , and ethanol, $\text{C}_2\text{H}_5\text{OH}$, (volume ratio 1 : 4) at 20 V during 2 min, to reduce surface roughness and create nanopatterns for posterior pore nucleation [28]. Finally, the substrates were rinsed in ethanol, followed by deionized water and dried in air.

In order to fabricate highly vertically oriented PAA templates a two-step anodization process was used [29]. First anodizations were carried out in 0.3 M oxalic acid, $(\text{COOH})_2$, at 40 V and 2 $^{\circ}\text{C}$, during 24 h, using a Keithley 2400 power supply. The formed alumina template was then removed in a mixture of 0.4 M phosphoric acid, H_3PO_4 , and 0.2 M chromic acid, H_2CrO_4 at 70 $^{\circ}\text{C}$ for 12 h. A second anodization was performed with the same conditions as the first one with a rate of $\sim 42 \text{ nm min}^{-1}$. For the individual studies the template thickness was chosen to be 10 μm . Immediately before electrodeposition, δ_b was reduced by applying an exponentially decreasing voltage from 40 V down to the desired potential [10].

A sequence of three different pulses was applied using a Keithley 2400 power supply. Firstly, a negative current density ($10\text{--}510 \text{ mA cm}^{-2}$) is applied for 8 ms to deposit the metal inside the PAA pores. Then a discharge pulse is applied for 2 ms with a voltage corresponding to the last applied potential drop of the δ_b defined in the barrier layer thinning process. This positive polarization pulse discharges the capacitance of the barrier layer and interrupts the electric field at the deposition interface after each deposition pulse. It has been further reported that this pulse repairs discontinuities in the barrier layer and improves its homogeneity [8]. Finally, a rest pulse is applied allowing repositioning the ions in the deposition interface. The electrolyte used was a mixture of $x \text{ g L}^{-1}$ iron(II) sulfate heptahydrate, $\text{FeSO}_4 \cdot 7\text{H}_2\text{O}$, 45 g L^{-1} boric acid, H_3BO_3 and 1 g L^{-1} ascorbic acid, $\text{C}_6\text{H}_8\text{O}_6$, where x was systematically varied between 2.78 g L^{-1} and 278 g L^{-1} . The pH value of the electrolyte was maintained at 2.4–3.0.

The factors considered to optimize the Fe PED were the electrolyte molar concentration (C), temperature (T) and stirring (S), rest pulse duration (t) and deposition pulse current density (j) and δ_b with standard values of 0.43 M, 20 $^{\circ}\text{C}$, 0 rpm, 0.7 s, 70 mA cm^{-2} and 10.4 nm, respectively [8–10, 19, 27, 30]. Given the large number of factors, statistical methods were employed to reduce the number of experiments necessary to understand the influence and cross influence of the variables. Response surface methods (RSMs) are a combination of statistical design of experiments tools effective to study responses via sophisticated optimization models [31]. The RSM analysis was achieved with JMP 9 software [32] using a central composite design (CCD) to fit second-order polynomials, which represent the effect of the operating conditions on the process response. The model parameters were obtained by the least square method [33] and are represented in table 1 together with their levels.

Table 1. CCD values and respective levels

Factor	Level		
	-1	0	1
<i>C</i> (M)	0.01	0.5	1
<i>T</i> (°C)	5	20	40
Stirring (rpm)	0	100	200
<i>t_r</i> (s)	0.3	0.7	1.2
<i>δ_b</i> (nm)	4	10	17
<i>j</i> (mA cm ⁻²)	10	75	125

PED was monitored using a Keithley 2400 power supply connected to a personal computer by a GPIB interface. A QUANTA-FEI field emission scanning electron microscope (FE-SEM), was used to evaluate the filled percentage (f_p) of the samples after ion milling (~ 500 nm) to remove the excess of material deposited on top of the PAA template. For each sample at least three different top areas were analyzed to obtain a more representative f_p value. The mean value and deviation are represented in the figures. The statistical count of f_p was performed using open source software for image analysis [34]. In each sample, three randomly selected regions of the surface were observed to infer a representative f_p . The template thickness of each sample was determined by cross section FE-SEM images. The samples were folded up to 180° to break the PAA template and the cracks were observed. The crystalline structure of the samples was analyzed by x-ray diffraction (XRD) in a Siemens Bruker AXS D5000 diffractometer in the θ - 2θ geometry using the Cu $-\text{K}\alpha$ line with wavelength $\lambda = 1.54 \text{ \AA}$. The magnetic measurements were performed in a commercial (Quantum Design) superconducting quantum interference device (SQUID) magnetometer, with sample reciprocating option, allowing very precise measurements 10^{-7} emu.

3. Results and discussion

The study of the deposition parameters was performed in two steps: first an experimental individual study of each parameter to understand its direct influence on the deposition quality; then, a cross influence of the parameters was studied through RSM.

3.1. Electrolyte molar concentration

The electrodeposition was carried out in an iron (II) sulfate bath, as it produces deposits that are smooth and can be operated at room temperature, in contrast with the ferrous chloride-calcium chloride bath [11]. As reported by Gadad et al [35] the use of Fe^{2+} electrolytes without H_3BO_3 leads to deposits containing significantly higher amounts of oxygen. Also, H_3BO_3 can act as a buffer to the hydrogen generation at the cathode, increasing the smoothness, compactness and continuity of the NWs [1, 36, 37].

Since in nanopore structures, the electrodeposition is diffusion limited according to Fick's law [37], the bulk molar concentration of $\text{FeSO}_4 \cdot 7\text{H}_2\text{O}$ was varied in the range of 0.01 to 1 M, in order to study the influence of Fe^{2+} concentration in the electrodeposition efficiency. Figure 1(a) shows the initial electrodeposition potential measured during the first electrodeposition pulse (8 ms), which corresponds to the deposition of the first metallic atomic layers at the pore bottom (V_0)

as a function of C . As the concentration of the electrolyte increases, an initial steady decrease of V_0 is visible, from 26 V for 0.01 M to 8 V for 0.25 M. In this range there are not sufficient ions for a uniform deposition and a higher potential needs to be applied to increase the electric field assisted diffusion in order to maintain the fixed current density. This potential corresponds to the applied bias to fix the current density at a predefined value. It can be seen that the potential increases with the solution concentration decrease. When an iron ion reaches the interface of the alumina barrier it is reduced to metal iron and the electron transfer allows for the current to flow. To have a constant current density, a certain potential needs to be applied to reduce the ions and overcome the thin insulator alumina layer. If there are not sufficient available ions to be reduced the potential starts to increase to force the electrons through the system and maintain the current density. As the potential increases, so does the electric field felt by the solution and the iron ions start to drift according to the electric field, thus aiding the diffusion, which will increase the ion concentration near the barrier layer. In this regime, the ionic concentration is rapidly depleted near the pore bottom and the growth is less compact following the electric field direction (vertical) instead of a more homogeneous growth given by a typical diffusion-controlled process [37, 38]. These irregularities in the NWs morphology during their growth reflect on lower f_p values (<50%), as shown in figure 1.

As the ionic species concentration increases, the electrodeposition becomes a diffusion-controlled process and the deposits are smooth and compact. Figure 1 shows an optimum range of C values is then observed between 0.25 M and 0.75 M, with a f_p maximum of 92% at 0.5 M. For higher C values (third regime, figure 1; above 0.8 M) the decrease in f_p can be attributed to the solubility of Fe-O-H being exceeded more easily, associated with the oxides formation, and hydrogen evolution [5, 35]. The pores are then blocked, causing an inefficient electrolyte renewal at the electrolyte/NW interface and the deposition efficiency decreases. The obtained experimental results can be observed in the SEM images (figure 1(b)).

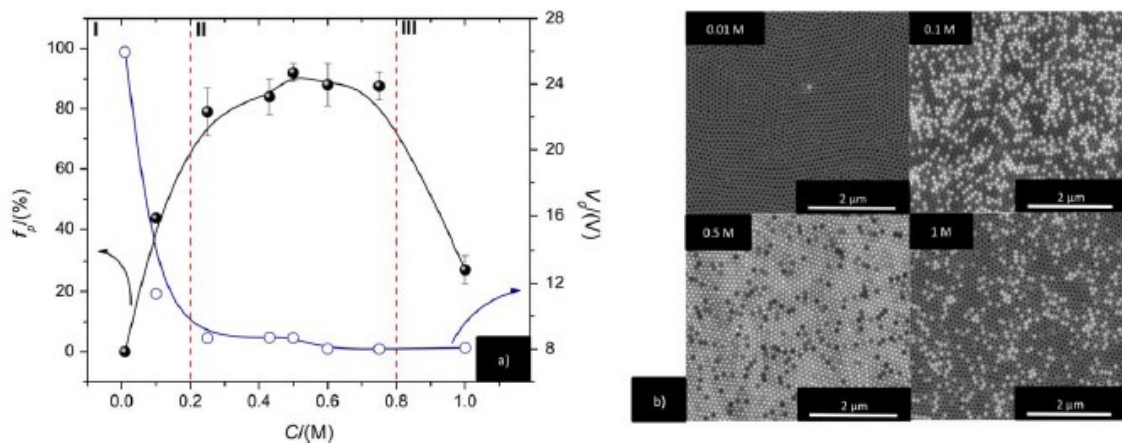


Figure 1. (a) Effect of $\text{FeSO}_4 \cdot 7\text{H}_2\text{O}$ concentration on f_p and V_0 . The PED parameters used are the standard values (T , S , tr , j and δ_b of 20 °C, 0 rpm, 0.7 s, 70 mAcm^{-2} and 10.4 nm, respectively). The solid lines are a guide to the eye. (b) Surface SEM images of samples electrodeposited at 0.01 M, 0.1 M, 0.5 M and 1 M.

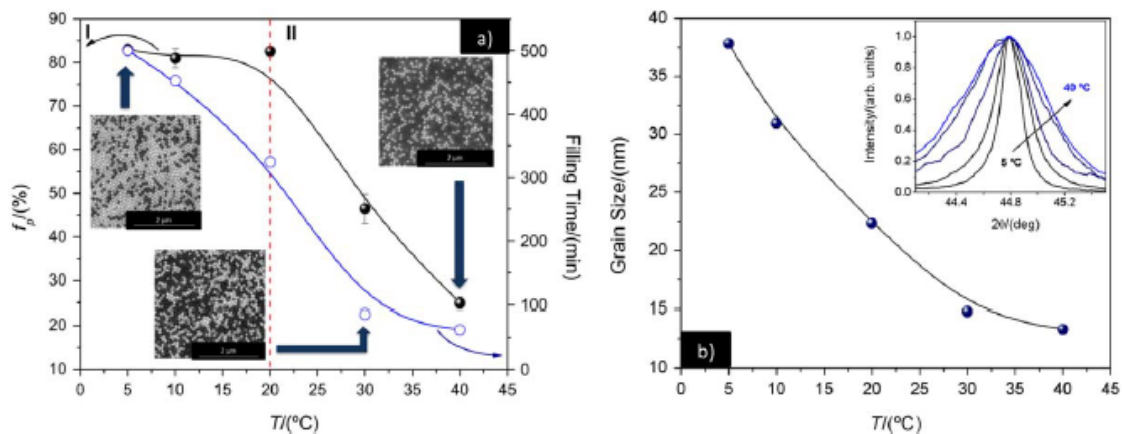


Figure 2. (a) f_p and filling time dependence on electrodeposition temperature with corresponding surface SEM images. The PED parameters used are the standard values (C , S , t_r , j and δ_b of 0.43 M, 0 rpm, 0.7 s, 70 mAcm⁻² and 10.4 nm, respectively). The solid lines are a guide to the eye; (b) Grain size versus temperature and Fe (110) Bragg diffraction peak (inset) for different electrodeposition temperature. Error bars contained within experimental points. The solid line is a guide to the eye.

3.2. Temperature

Deposition temperature is one of the key features to obtain highly uniform growth of the NWs [5, 38, 39], so the effect of deposition temperature (between 5 and 40 °C) in f_p was here also studied. For temperatures below 5 °C the solution precipitated very quickly, covering the PAA surface and thus inhibiting the deposition, while for $T > 40$ °C a strong H₂ evolution was observed which hinders the electrodeposition, especially if the formed gas bubble are large enough to completely block the pores.

The f_p values, for different temperatures, are presented in figure 2(a), together with the electrodeposition time at which a film started to be deposited on the surface of the PAA membrane (filling time). The electrodeposition rate (figure 2(a)) increases for temperatures above 20 °C (for 40 °C it is 5 times faster than for 20 °C), but the lower f_p values beyond this point indicate an irregular NW growth.

It is clearly seen that the overall f_p of the Fe NWs is significantly enhanced as the deposition temperature is decreased down to 2 °C. These low temperatures lead to a slow ion diffusion (Einstein–Stokes equation [40]) inside the PAA pores and consequently reduce the heterogeneity of NW growth [22, 38, 41]. Therefore, below the 20 °C threshold the deposition is smooth and regular and f_p reaches a stable value around 80% (regime I, figure 2). However, this stability is related with the balance between the high length uniformity and electrolyte precipitation that for temperatures below 5 °C starts to inhibit electrodeposition.

Ion diffusion speed increases with temperature and so does the deposition rate (see figure 2 (a)). As ions are more readily available in the cathode, native defects in the alumina barrier will have major influence in the electrodeposition given that the deposition is no longer diffusion limited. Small imperfections in the alumina barrier and pore structure along the PAA template lead to different local current densities and a heterogeneous material deposition [42]. Therefore, the faster growing pores eventually reach the top of the template and block their

neighbors by growing over the adjacent pores in a mushroom-like structure [23], leading to f_p values as low as 25%. The heterogeneous j distribution can be verified by XRD measurements where high temperatures produce smaller grain sizes, associated with higher j [figure 2(b); determined using the Scherrer's equation] [27].

3.3. Stirring

We tested the influence of stirring in f_p and V_0 , by introducing a teflon fan in the electrolyte solution and turning it at different rpm (figure 3). This way the bulk electrolyte outside the PAA was stirred. For low stirring velocities (regime I, figure 3), f_p values are high ($\sim 80\%$) with average $V_0 = 10.2$ V. However, when one increases the stirring velocity above 50 rpm, V_0 increases and f_p decreases abruptly (from 80% to 0%).

To our knowledge, the influence of stirring on the deposition quality in PAA templates has never been studied. Although it was expected that stirring would benefit the homogenization of the electrolyte, thus improving the electrodeposition quality, in the case of electrodeposition inside the PAA pores it is clear that stirring has a negative effect. Ren et al [41] reported the same behavior for the electroplating of Ni thin films. They argued that Ni was electrodeposited in several steps with the intermediate formation of adsorbed Ni(OH). With stirring, the admission of H^+ is hindered, creating conditions for the accumulation of adsorbed Ni(OH). The same thing is likely to be occurring in our experiments, as Fe electrodeposition is believed to also proceed in a two-step process with the intermediate formation of adsorbed Fe(OH) [35]. Further studies should be made to completely understand the influence of stirring in the electrodeposition of Fe in PAA templates.

For very high stirring speeds, the hydrodynamic conditions at the alumina surface become irregular and the rotation is strong enough to deplete the electrolyte in the center of the sample so that only the outer areas were filled, although at low f_p .

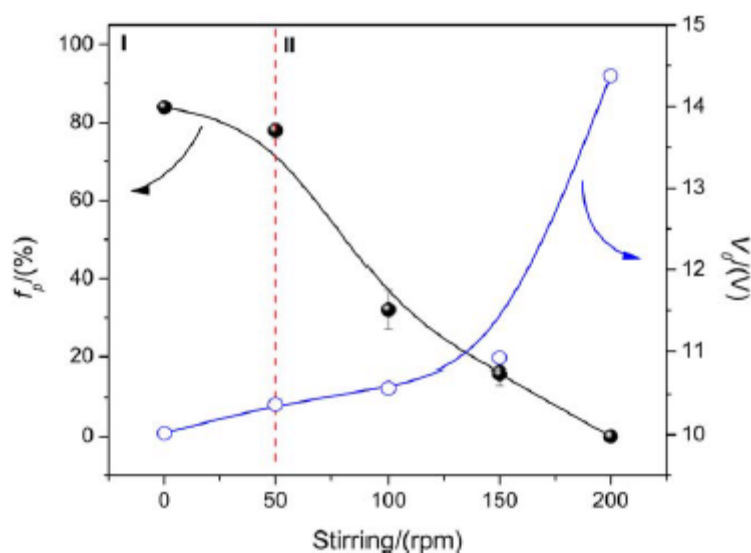


Figure 3. Dependence of f_p and V_0 on stirring velocity. The PED parameters used are the standard values (C , T , t_r , j and δ_0 of 0.43 M, 20 °C, 0.7 s, 70 mA cm⁻² and 10.4 nm, respectively). The solid lines are a guide to the eye.

3.4. Rest pulse duration

It is essential to ensure the presence of enough ions to be reduced at the pores bottom to guaranty a good deposition quality and the rest pulse allows the renewal of the concentration of Fe^{2+} ions inside the PAA pores after each deposition pulse. Its influence was studied in detail elsewhere [27] and is here only briefly described. Two different regimes were observed (figure 4), the first corresponding to insufficient rest pulse duration for a complete concentration recovery and the second to an overexposure to the electrolyte, promoting an accentuated chemical attack (decreasing f_p trend with t_r). The maximum f_p was observed at $t_r = 0.6$ s with 91.9% pores filled.

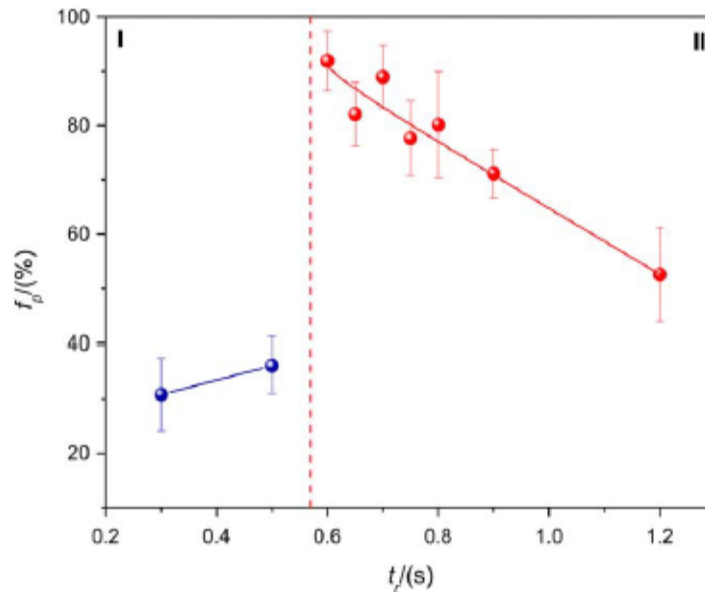


Figure 4. Dependence of f_p with t_r . The PED parameters used are the standard values (C , T , S , j and δ_b of 0.43 M, 20 °C, 0 rpm, 70 mAcm^{-2} and 10.4 nm, respectively). The solid line is a guide to the eye.

3.5. Barrier layer thickness

The bottom layer thickness determines the electron flow during electrodeposition, that enables the ion reduction and consequent deposition. We therefore studied the influence of δ_b on the Fe NWs deposition quality by varying the barrier layer thickness from 4 to 17 nm (corresponding to 3 V and 13 V, respectively).

Figure 5(a) shows the deposition curves for different samples, where the maximum potential value in each curve (corresponding to the final stage of ramifications filling) is marked (t_d). For very low δ_b , the electric current distribution in the PAA pores is very sensitive to small thickness variations. Then, a small portion of the pores will be supplied with enough current to rapidly grow, reaching the top of the template and blocking the neighboring ones. This can be observed in figure 5(a) where, for $\delta_b = 3.9$ nm, the potential is still increasing (dendritic filling of the slow growing NWs) when the typical noise corresponding to the deposition on top of PAA appears (rapidly growing NWs).

For high δ_b values, the resistance that the alumina barrier offers the electron flow is increased. Thus, upon a constant j pulse and given the fluctuations in the thickness of the oxide layer, some pores suffer dielectric breakdown and j is immediately distributed to the resulting low resistance channels. Contrarily to the low δ_b value cases, this time only a few pores will actually start to fill, although at very high rates, giving rise to low t_d values. Since δ_b has random fluctuations, the f_p values largely vary from site to site, as observed in different surface areas of the same sample by SEM, inserting an associated error in the measurements. Figure 5(b) shows f_p as a function of δ_b , where an optimum regime ($8 \text{ nm} < \delta_b < 10 \text{ nm}$) is observed with $f_p \sim 85\%$, below and above which it declines abruptly. These results are in good agreement with previous studies for Ni NWs, where an optimum value was observed at $\sim 10 \text{ nm}$ [10].

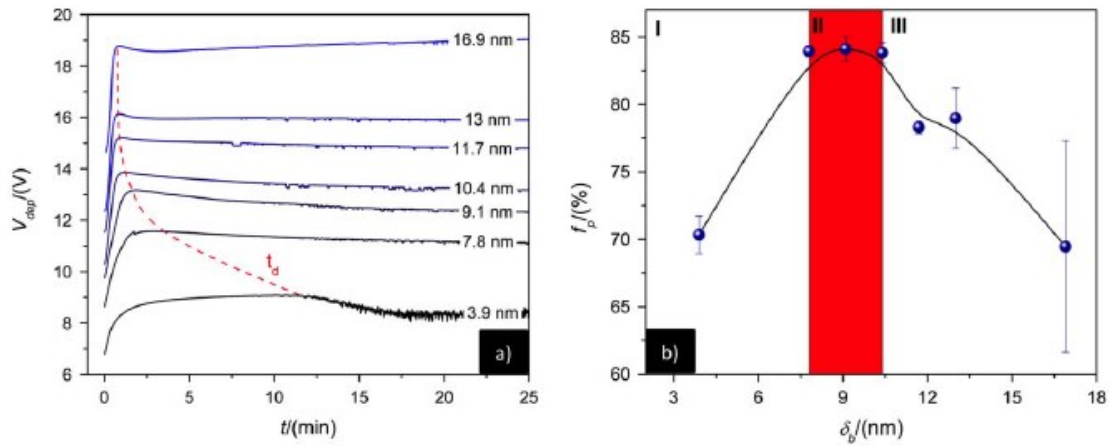


Figure 5. (a) Deposition profiles for different δ_b and corresponding dendrites filling times (t_d); (b) Dependence of f_p with δ_b . The PED parameters used are the standard values (C , T , S , t_r , j of 0.43 M, 20 °C, 0 rpm, 0.7 s and 70 mAcm⁻², respectively). The solid lines are a guide to the eye.

3.6. Deposition pulse current density

The applied j during the deposition pulse will determine the number of available electrons to reduce the Fe²⁺ ions in the electrolyte. Hence, it will also establish the deposition rate and concentration depletion at the end of each deposition pulse. Furthermore, it is a crucial parameter to obtain a good barrier layer stability and prevent dielectric breakdowns. Therefore a set of j values was tested, ranging from 10 to 510 mA cm⁻².

Figure 6(a) shows deposition profiles at different j values. The time that it takes for the NWs to reach the top of the template decreases with increasing j , as the rate of Fe reduction is enhanced, being also very clear in the first stages of deposition (inset). In figure 6(b) we observe that V_0 follows the expected linear relation with j (Ohm's law) from low j values up to 125 mA cm⁻² (low j regime). Since every experiment was conducted in the same conditions, the reproducibility of the quality of the template can be evaluated from this result, as the resistivity of the barrier layer and electrolyte remains constant [42]. For higher j , deviations from the linear trend are observed.

The f_p for different j values is presented in figure 7(a). The existence of the two different regimes is here also clear, with a threshold at 125 mA cm⁻². In the low j regime a rapid increase of the filling percentage from $f_p \sim 20\%$ (at 40 mA cm⁻²) to $f_p > 90\%$ (at 70 mA cm⁻²) is seen. Above this value a saturation is reached with a maximum of $f_p = 95\%$ encountered for 117 mA cm⁻². For j

higher than 125 mA cm^{-2} , f_p presents a random behavior and low reproducibility. Nevertheless, an overall increasing tendency is observed, from f_p of 12% to 93% at 152 mA cm^{-2} and 510 mA cm^{-2} , respectively.

In the low j regime, one expects that with increasing current, more pores are filled since electrons are readily available. For very low currents, f_p is also low as the deposition is slow and template exposure to the electrolyte also increases, affecting the deposition quality. As j increases, the deposition becomes more regular as the majority of the pores receive enough current for a good homogeneous growth. A saturation regime is observed from 70 to 125 mA cm^{-2} , with a maximum $f = 94\%$, given that the depletion of Fe^{2+} at the pores bottom becomes a predominant factor as j increases, i.e. more electrons are available for the reduction reaction but there are no ions to be reduced.

For high j values, several factors start to become predominant, such as pH fluctuations, H_2 evolution and even dielectric breakdown in the alumina barrier due to excessive local current [8, 16]. In these situations, given the heterogeneity between pore impedances [42], the current distribution will be uneven and a preferential growth in a fraction of the template is observed. The lower limit of this regime presents the lowest f_p . It is the point where dielectric breakdown occurs in the barrier layer creating low resistance channels for the electrons to flow, limiting the current access in most of the PAA pores. As j increases, so does the number of pores that suffer dielectric breakdown and that will be efficiently deposited, thus the rising trend. Since the alumina barrier layer is the major resistive component (by three orders of magnitude) [42], very small variations in δ_b will have a major impact in the j distribution. Thus, dielectric breakdown depends on the fluctuations in δ_b , giving rise to the large error bars. This is also observed in the V_0 variations shown in figure 6(b) which are due to the random nature of the pore bottom dielectric breakdown distribution in the PAA membrane. When extremely high j values are used most of the pores suffer a breakdown and higher f_p are observed.

The previous conclusions are supported by a grain size analysis. The increase of j in the low j regime leads to a smooth decrease of the grain size (figure 7(b)) [43]. However, in the high j regime the grain size does not follow any definitive trend. The high j values used and consequent dielectric breakdown of the barrier layer lead to non-homogeneous current distributions and different local j -values, during pore filling, compared to the nominal value due to the fluctuations in the nominal thickness of the barrier layer.

From magnetic measurements, we were also able to obtain the saturation moment of each sample and, combined with the deposition total time, to determine the deposition rate of $0.34 \text{ ng cm}^{-2} \text{ s}^{-1} \cdot \text{mA}$.

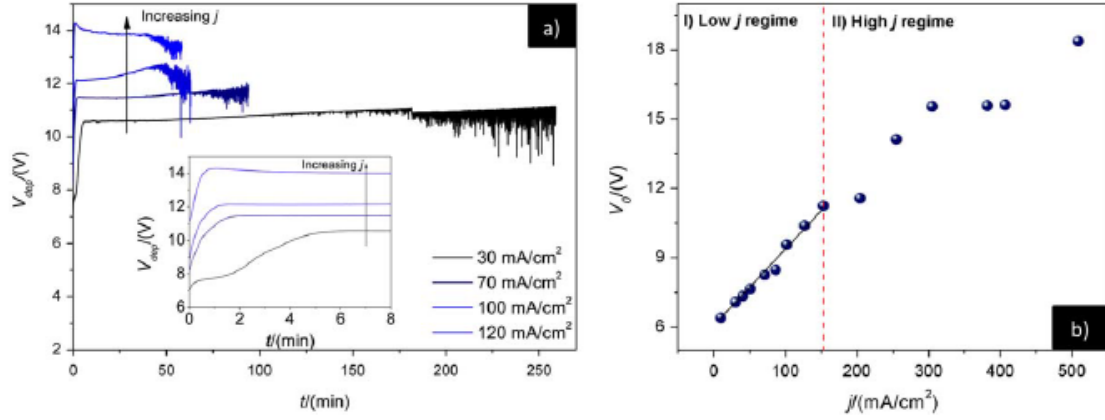


Figure 6. (a) Deposition profiles, with increasing j , taken during electrodeposition (initial stages are shown in detail in the inset); (b) V_0 dependence on j . The PED parameters used are the standard values (C , T , S , t_r , and δ_b of 0.43 M, 20 °C, 0 rpm, 0.7 s and 10.4 nm, respectively).

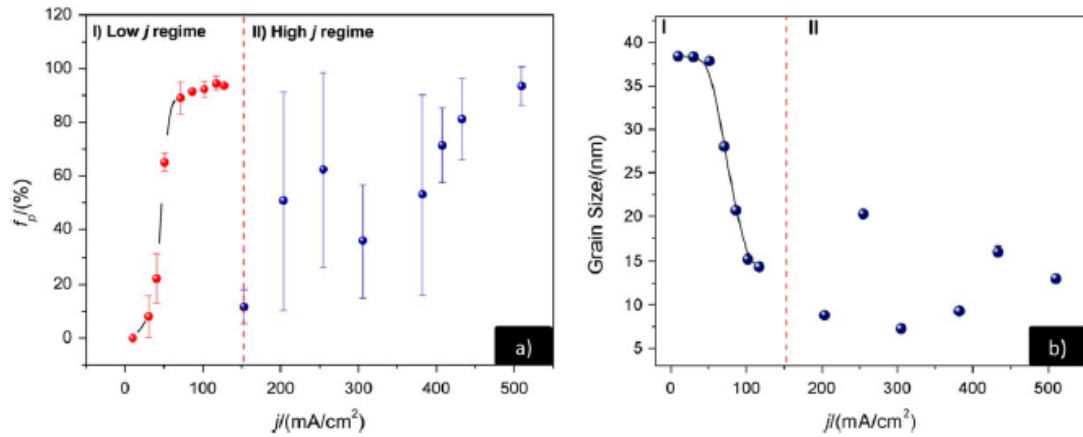


Figure 7. (a) Filled percentage dependence on the current density; (b) Grain size versus j . Error bars contained within experimental points. The PED parameters used are the standard values (C , T , S , t_r , and δ_b of 0.43 M, 20 °C, 0 rpm, 0.7 s and 10.4 nm, respectively). The solid lines are a guide to the eye.

Table 2. Optimum electrodeposition parameters obtained from RSM analysis and experimental results.

Parameter	RSM Analysis	Individual Experimental Results
δ_b (nm)	9.1	9
Stirring, (rpm)	0	0
t_r (s)	0.82	0.6
j (mA cm ⁻²)	94	125
C (M)	0.55	0.5
T (°C)	12	20

3.7. Cross parameter influence

After understanding all the primary effects of the electrodeposition parameters, a response surface methodology was implemented to assess the optimum set of parameters for a complete PAA filling. In this work, a central composite design (CCD) was selected as it is the most used method to fit second-order models [27]. As mentioned previously, optimum variable ranges were pre-selected to enhance the precision of the statistical method. For 6 factors and 2 central points the CCD method indicates 46 runs.

From the analysis of variance (ANOVA) of the model, it was verified that all model parameters p-values are smaller than 0.005 making their contribution for the response of the system significant. An optimum set of deposition conditions was determined and is presented in table 2, together with the optimum experimental conditions, obtained from the previous individual studies. The statistical trends for each parameter are represented in figure 8 corresponding to a maximum statistical value of f_p ($104 \pm 12\%$).

The maximum of f_p is predicted to occur for parameters values given in table 2. The optimum values obtained from the individual studies are in accordance with the RSM analysis, which was expected. With these optimum sets of parameters, the limits of f_p were tested for different template lengths and compared with the initial reference values (figure 9(a)). For lengths up to 20 μm the PAA is filled up to 93%. For higher lengths, f_p steadily decreases down to 77% for 50 μm length. Nevertheless, the growth of the NWs remains highly homogeneous very close to 50 μm as can be seen in the cross section image of a 50 μm sample (figure 9(b)). In the last few micrometers of the template, as the first NWs reach the surface of the template, they start to cover the adjacent pores preventing a complete template filling (figure 9(c)). Although for low thicknesses the nominal f_p values are similar in all the used sets of parameters, as the PAA length increases it is noteworthy the improvement in the deposition homogeneity for the RSM results. Using the best deposition parameters we eliminated the pore blocking problems that arise in the last few micrometers. A 55 μm template was used and the last 5 μm were milled after deposition to study the growth homogeneity in 50 μm length. The result is presented in figure 9(a) by a red star, with an f_p of 89%. The SEM image can be observed in figure 9(d), this being the highest filling ratio reported for ac or PED methods, opening a new window of opportunities for the fast fabrication of long, organized NWs.

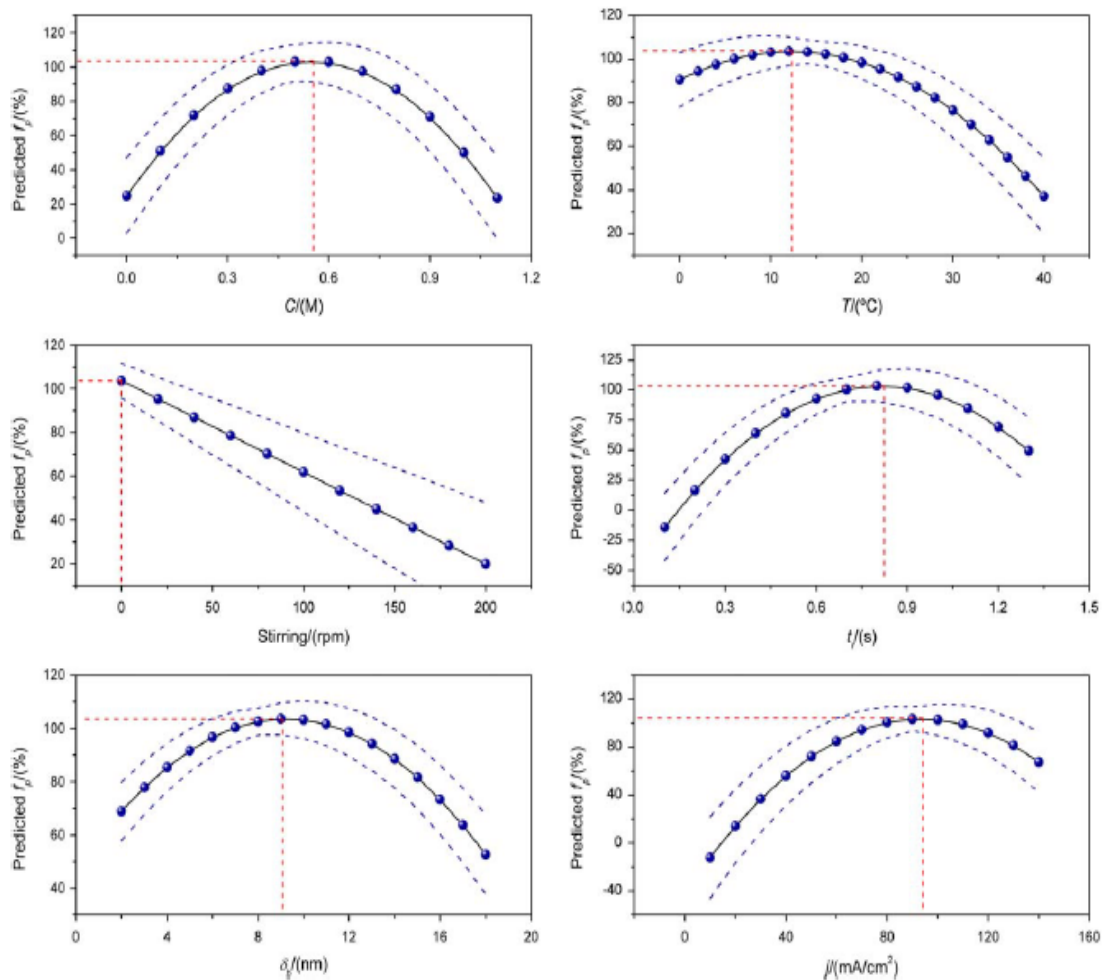


Figure 8. Prediction profiles for each studied electrodeposition parameter and corresponding confidence intervals (blue dashed lines). For each parameter, the desirability plot is presented under the prediction profile. The solid lines are a guide to the eye and the dashed lines represent the confidence intervals.

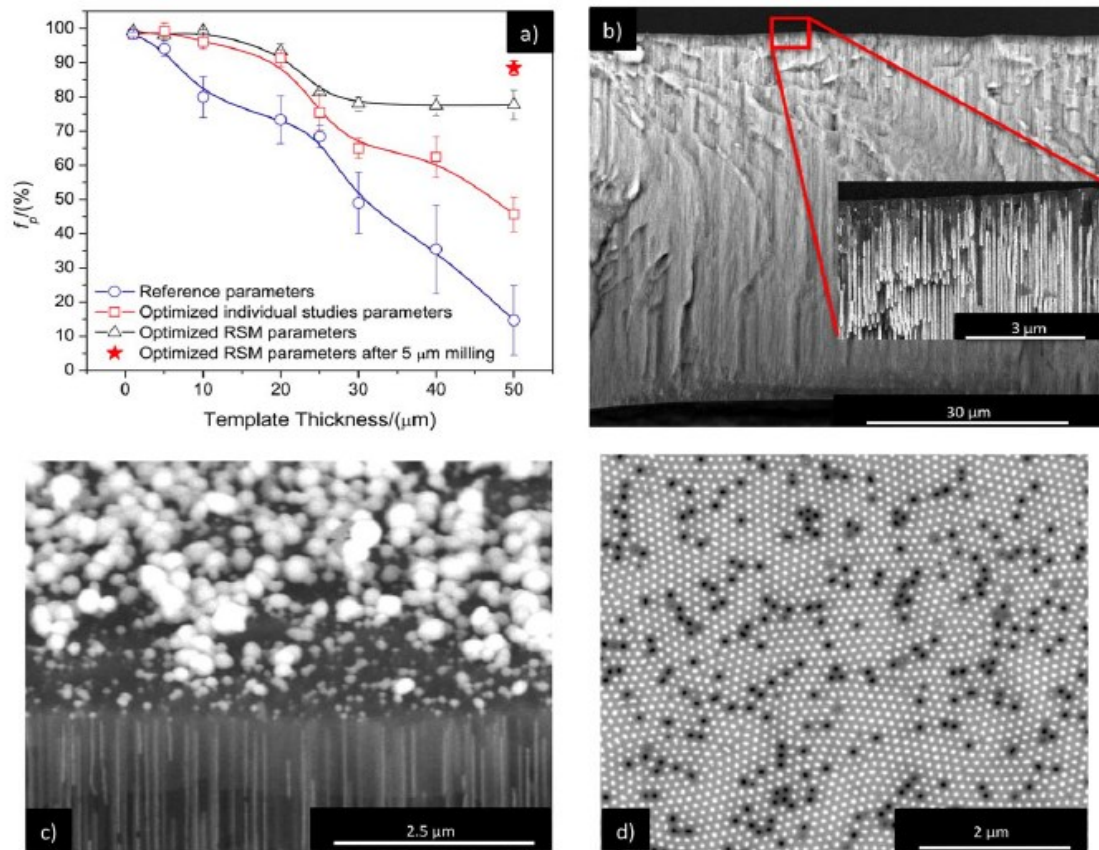


Figure 9. (a) Filled percentage dependence on template thickness for reference, optimized from individual studies and RSM optimized parameters. The solid line is a guide to the eye; (b) SEM cross section image of a 50 μm PAA filled sample; (c) top view without milling: the white mushroom structures correspond to the deposits once the nanowires reach the template surface; (d) SEM top view image of a 50 μm PAA filled sample after 5 μm milling.

4. Conclusions

In this work, we show for the first time the application of the pulsed electrodeposition as the simplest method to fabricate vertically aligned iron nanowire arrays with extreme homogeneity up to 50 μm . We performed a systematic study on the influence of several pulsed electrodeposition parameters in the deposition quality of Fe nanowires. The results reveal that electrolyte molar concentration, temperature, stirring, rest pulse duration, barrier layer thickness and current density have significant impact on f_p . Each parameter was investigated and optimized from an initial set of reference values.

We show the importance of a cross parameter optimization to achieve very thick homogeneous nanowire arrays, something that was not shown before. With an RSM analysis the optimum set of values was predicted as follows: barrier layer thickness of 9.1 nm, 0 rpm stirring, rest pulse duration of 0.82 s, deposition pulse current density of 94 mA cm^{-2} , electrolyte molar concentration of 0.55 M and temperature of 12 $^{\circ}\text{C}$. With this set of parameters, highly homogeneous filled templates were obtained with f_p up to 93% for 20 μm . Also, high filling ratios are reported for very thick templates (50 μm) using alternate current methods. It is the first report of such excellent homogeneities in alternating current reports, for iron or any material.

Acknowledgments

Work supported in part by project PTDC/EQU-EQU/115614/2009 and PTDC/EQU-EQU/107990/2008. J Azevedo and C T Sousa are grateful to FCT SFRH/BD/79207/2011 PhD grant and postdoctoral grant SFRH/BPD/82010/2011, respectively. J Ventura acknowledges financial support through FSE/POPH. A Apolinario acknowledges financial support through PTDC/EQU-EQU/107990/2008 and PTDC/CTM-MET/118236/2010. The authors also acknowledge operation NORTE-070124-FEDER-000070—Multifunctional Nanomaterials funded by FEDER and CCDRN.

References

- [1] Borissov D, Isik-Uppenkamp S and Rohwerder M 2009 *J. Phys. Chem. C* 113 3133–8
- [2] Jagminas A, Mažeika K, Reklaitis J, Pakštas V and Baltrūnas D 2009 *Mater. Chem. Phys.* 115 217–22
- [3] Yang S, Zhu H, Yu D, Jin Z, Tang S and Du Y 2000 *J. Magn. Magn. Mater.* 222 97–100
- [4] Cornejo D R and Padrón-Hernández E 2007 *J. Magn. Magn. Mater.* 316 48–51
- [5] Haehnel V, Fähler S, Schaaf P, Miglierini M, Mickel C, Schultz L and Schlörb H 2010 *Acta Mater.* 58 2330–7
- [6] Sun M, Zangari G, Shamsuzzoha M and Metzger R M 2001 *Appl. Phys. Lett.* 78 2964–6
- [7] Santos A, Vojkuvka L, Pallarés J, Ferré-Borrull J and Marsal L F 2009 *Nanoscale Res. Lett.* 4 1021–8
- [8] Nielsch K, Muller F, Li A and Gosele U 2000 *Adv. Mater.* 12 582–6
- [9] AlMawlawi D, Coombs N and Moskovits M 1991 *J. Appl. Phys.* 70 4421–5
- [10] Sousa C T, Leitao D C, Proença M P, Apolinário A, Correia J G, Ventura J and Araújo J P 2011 *Nanotechnology* 22 315602-7
- [11] Schlesinger M 2011 *Modern Electroplating* (New York: Wiley)
- [12] Vrublevsky I, Jagminas A, Schreckenbach J and Goedel W A 2007 *Appl. Surf. Sci.* 253 4680–7
- [13] Mao A, Han G Y and Park J H 2010 *J. Mater. Chem.* 20 2247–50
- [14] Ji C and Searson P C 2003 *J. Phys. Chem. B* 107 4494–9
- [15] Li L, Pan S, Dou X, Zhu Y, Huang X, Yang Y, Li G and Zhang L 2007 *J. Phys. Chem. C* 111 7288–91
- [16] Proença M P, Sousa C T, Ventura J, Vazquez M and Araujo J P 2012 *Electrochim. Acta* 72 215–21
- [17] Qin J, Nogués J, Mikhaylova M, Roig A, Muñoz J S and Muhammed M 2005 *Chem. Mater.* 17 1829–34
- [18] Kalska-Szostko B, Brancewicz E, Mazalski P, Sveklo J, Olszewski W, Szymanski K and Sidor A 2009 *Acta Phys. Pol. A* 115 542-4

- [19] Baik J M, Schierhorn M and Moskovits M 2008 J. Phys. Chem. C 112 2252–5
- [20] Gerein N J and Haber J A 2005 J. Phys. Chem. B 109 17372–85
- [21] Lee J, Farhangfar S, Lee J, Cagnon L, Scholz R, Gösele U and Nielsch K 2008 Nanotechnology 19 365701–9
- [22] Trahey L, Becker C R and Stacy A M 2007 Nano Lett. 7 2535–9
- [23] Sousa C T, Apolinário A, Leitao D C, Pereira A M, Ventura J and Araújo J P 2012 J. Mater. Chem. 22 3110-6
- [24] Meng G, Jung Y J, Cao A, Vajtai R and Ajayan P M 2005 Proc. Natl. Acad. Sci. 102 7074–8
- [25] Cheng W, Steinhart M, Gösele U and Wehrspohn R B 2007 J. Mater. Chem. 17 3493–5
- [26] Nielsch K, Choi J, Schwirn K, Wehrspohn R B and Gösele U 2002 Nano Lett. 2 677–80
- [27] Azevedo J, Sousa C T, Mendes A M and Araújo J P 2012 J. Nanosci. Nanotechnol. 12 9112–7
- [28] Leitao D C, Apolinario A, Sousa C T, Ventura J, Sousa J B, Vazquez M and Araujo J P 2011 J. Phys. Chem. C 115 8567-72
- [29] Masuda H and Fukuda K 1995 Science 268 1466–8
- [30] Peng Y, Zhang H L, Pan S L and Li H L 2000 J. Appl. Phys. 87 7405–8
- [31] Anderson M J and Whitcomb P J 2004 RSM Simplified: Optimizing Processes Using Response Surface Methods For Design of Experiments (University Park, IL: Productivity, Inc.)
- [32] JMP9 1989–2007 SAS Institute Inc. <http://www.jmp.com/>
- [33] Catarino M, Ferreira A and Mendes A 2009 J. Membrane Sci. 341 51–9
- [34] ImageJ 1997–2011 US National Institutes of Health <http://imagej.nih.gov/ij/>
- [35] Gadad S and Harris T 1998 J. Electrochem. Soc. 145 3699–703
- [36] Zech N and Landolt D 2000 Electrochim. Acta 45 3461–71
- [37] Schlörb H, Haehnel V, Khatri M S, Srivastav A, Kumar A, Schultz L and Fähler S 2010 Phys. Status Solidi (b) 247 2364–79
- [38] Shin S, Kong B H, Kim B S, Kim K M, Cho H K and Cho H H 2011 Nanoscale Res. Lett. 6 467–75
- [39] Ramírez D, Gómez H, Riveros G, Schrebler R, Henríquez R and Lincot D 2010 J. Phys. Chem. C 114 14854-9